Clio: A 5 micron camera for the detection of giant exoplanets

Melanie Freed[a], Philip M. Hinz[a], Michael R. Meyer[a], N. Mark Milton[a], and Michael Lloyd-Hart[a]

[a]Steward Observatory, 933 N. Cherry Ave, Tucson, AZ 85721, USA

ABSTRACT

We plan to take advantage of the unprecedented combination of low thermal background and high resolution provided by the 6.5m MMT's adaptive secondary mirror, to target the 3-5 micron atmospheric window where giant exoplanets are expected to be anomalously bright. We are in the process of building a 3-5 micron camera that we will use to carry out a survey to characterize the prevalence and distribution of giant planets around nearby, Sun-like stars. Sensitivity estimates show that for a 1 Gyr old G0V primary at 10 pc, we expect to detect 5 $M_{\rm Jupiter}$ and 15 $M_{\rm Jupiter}$ exoplanets at angular separations greater than 0.45-2.1" and 0.2-1.2" respectively. Monte Carlo simulations based on these sensitivity estimates and a sample of 80 young (<1 Gyr), nearby (<20 pc) M0V-F0V stars, predict the detection of 15±3 exoplanets with masses of 4-15 $M_{\rm Jupiter}$ and separations of 17-50 AU. Construction of the camera is currently underway and on-telescope testing is expected in the Fall 2004-Winter 2005.

Keywords: exoplanets, thermal infrared, imaging, adaptive optics

1. INTRODUCTION

With the number of known extrasolar planets now exceeding 100 (http://www.obspm.fr/encycl/catalog.html), we have reached the point where we can begin to study the statistical properties of these planets (e.g. Marcy et al. (2003)[1]). However, while radial velocity surveys have provided a wealth of information about exoplanets, they are unable to determine the inclination of the systems or obtain any spectral information about the exoplanets. In addition, they are limited to relatively small star-planet separations over a practical temporal baseline. Other indirect methods such as astrometry and microlensing are also valuable tools for the detection of exoplanets. However, only by direct detection can any spectral information about the exoplanets be determined, which is crucial to studying their physical properties (e.g. temperature, surface gravity, composition).

So far, the transit method is the only direct technique that has successfully detected exoplanets. The confirmation of the radial velocity planet HD209458b by transit techniques[2] led to the first detection of sodium in an exoplanetary atmosphere.[3] Since then, three additional transitting exoplanets have been discovered with the OGLE survey[4–6] While transit techniques clearly have the potential to provide a wealth of information about exoplanets, they are also limited to close in planets, where multiple transits can quickly be observed and exoplanets are more likely to transit their primary star.

In an effort to directly detect exoplanets at separations left largely unexplored by current measurements, we are building an imager, Clio, to be used in the thermal infrared with ground-based adaptive optics (AO). Cool exoplanets (T_{eff} < 1000 K) are thought to peak in brightness in the thermal IR from 3-5 microns (e.g. Burrows et al. (1997)[7]). Until now, it has been impossible to take high-resolution data in the thermal IR since no appropriate space-based telescope exists and the thermal background is so large from the ground. Additional emissivity introduced by conventional AO systems overwhelms any astronomical signal. With the MMT's adaptive secondary we can combine the thermal IR and high-resolution to help close the separation sensitivity gap between seeing-limited direct imaging surveys and indirect methods such as radial velocity surveys.

Further author information: (Send correspondence to M.F.)
M.F.: E-mail: freed@as.arizona.edu, Telephone: 1 520 626 8072

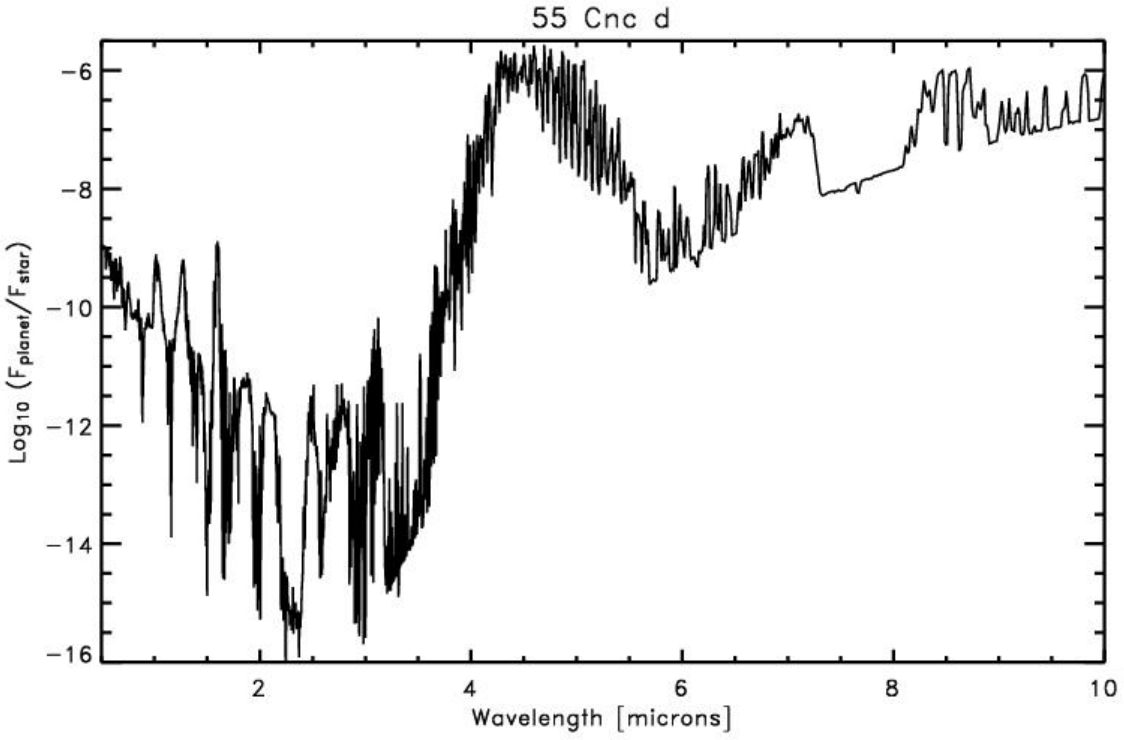

Figure 1. Theoretical contrast spectrum of 55 Cnc d from the equilibrium models of Sudarsky, Burrows, and Hubeny (2003).[11] 55 Cnc d is an exoplanet, discovered with radial velocity methods, orbiting a G8V primary star at 5.9 AU and has an assumed mass of 4.05 $M_{\rm Jupiter}$ and age of 5 Gyr.

2. EXOPLANET SPECTRA IN THE THERMAL INFRARED

Theoretical studies of both isolated and irradiated exoplanets with equilibrium models have shown that a strong peak in emission exists between 4 and 5 microns.[7–11] This 4-5 micron enhancement results from the combination of supressed flux longward of 10 microns by collision-induced absorption of H_2 and windows in the H_2O opacity spectrum. These two effects force flux blueward, producing large flux enhancements over blackbody values in the J, H, and M bands.[7] The cooler an object is, ($T_{eff} < 1000$ K), the larger this effect becomes. While J, H, and M band fluxes are all increased relative to their blackbody values, the M band stays brighter than both J and H bands as exoplanets become cooler and the Wein law blackbody quickly suppresses the bluer J and H bands. The fact that the M band flux stays brighter for cooler exoplanets makes it ideal for studies of companions around nearby stars, since they tend to be older.

However, a study by Golimowski et al (2004)[12] of 63 of M1-T9 dwarfs shows that their observed M′ flux is 1.5-2.5 times lower than the values predicted by equilibrium models. The non-equilibrium models ($700 \leq T_{eff} \leq 2000$ K) of Saumon et al. (2003)[13] are better able to reproduce the observed values as a result of an overabundance of CO due to the non-equilibrium chemistry. Vertical mixing in the models brings CO up from deeper stellar layers faster than it can be converted to CH_4. The larger CO abundance then produces stronger absorption from 4.5-5 microns. These results may indicate that the 4-5 micron enhancement may not be as strong in exoplanets as originally thought. More studies are necessary to estimate the magnitude of this effect for the exoplanets we are targetting ($T_{eff} < 700$ K). Figure 1 shows the equilibrium theoretical spectrum of 55 Cnc d (Sudarsky, Burrows, and Hubeny (2003)) including irradiation effects. This exoplanet orbits a G8V primary star at 5.9 AU and has an estimated mass of 4.05 $M_{\rm Jupiter}$ and age of 5 Gyr. Its properties are typical of the type of exoplanets that we expect to find at the limits of our sensitivity.

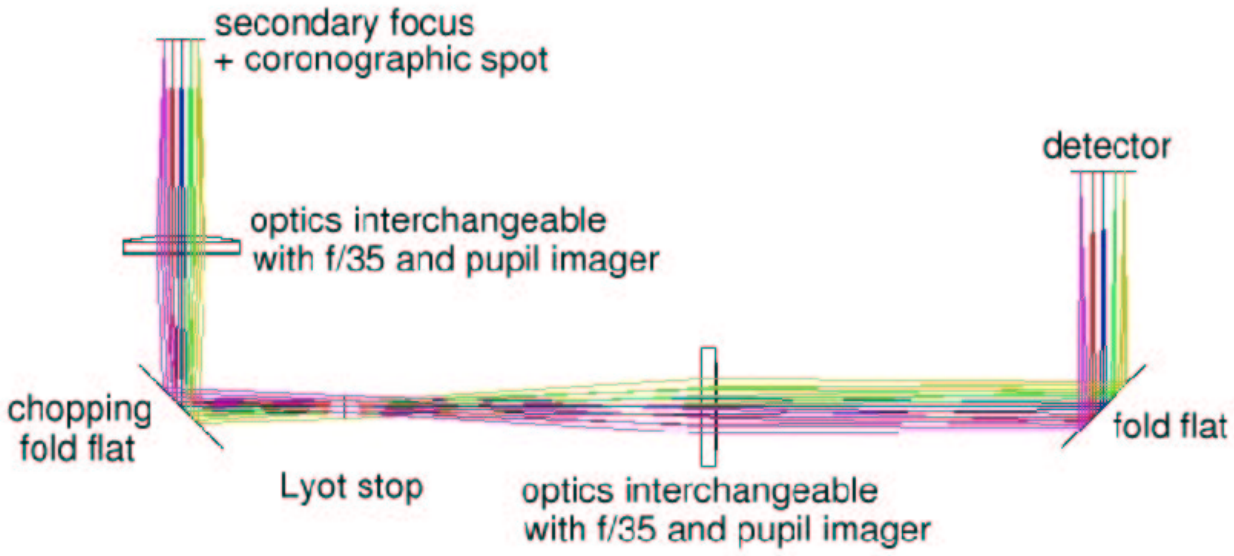

Figure 2. Optical drawing of the f/20 channel of Clio. The dewar window is not shown.

3. THE ADAPTIVE SECONDARY

While theoretical models predict that the 4-5 micron wavelength region may be an optimal place to search for exoplanets, high thermal background with AO from the ground has made such studies impractical. The adaptive secondary mirror at the 6.5m MMT provides a solution to the problem of increased emissivity from conventional AO systems. By making the secondary mirror of the telescope itself the deformable surface, approximately eight additional surfaces are eliminated compared to typical AO systems.[14] This results in both an emissivity and throughput that are similar to a non-AO equipped telescope. For faint objects, a conventional AO system at the MMT would require observations 2-3 times longer to reach sensitivity in the L and M bands comparable to the adaptive secondary system.[14]

The adaptive secondary mirror is now operational at the MMT telescope.[15,16] Measurements taken with the BLINC/MIRAC mid-IR camera indicate an emissivity of 6.5% for the telescope plus AO system, which is lower even than typical telescopes without AO. In January 2003, BLINC/MIRAC also recorded the first high order AO images taken in the thermal IR. These were taken at 10.3 microns and show an achieved Strehl ratio of 0.96 with the AO system operational. Once vibration-related issues are resolved, the adaptive secondary should be able to achieve a Strehl of 0.87 at M band. This number is based on short integration observations in the H-band with the vibrations removed in post-processing.

4. CLIO

4.1. Optical Design

Clio will be a three channel system that consists of f/20, f/35, and pupil imaging modes. The primary design driver for Clio is use in the high background regime (i.e. L and M bands). The f/20 channel has been optimized for the L and M bands with Nyquist sampling at L band (0.048"/pixel) and a field of view of 15 x 12". The f/35 channel is optimized for the H and K bands with Nyquist sampling at K band (0.027"/pixel) and a FOV of 8.7 x 7".

Figure 2 shows the optical design of the f/20 channel minus the dewar window. The dewar window is a dichroic that reflects light from 350-950 nm into the AO system and transmits light longward of 1 micron into the instrument. At the Cassegrain focus of the f/15 adaptive secondary, inside the dewar, a wheel will allow a selection of coronographic stops to be moved into the beam. Optics will then form an image of the secondary,

where another wheel will allow a selection of Lyot stops to be introduced into the beam before the final image is formed on the detector. An articulating fold flat near the pupil will enable modulation of the sky signal on the detector.

4.2. Detector

Clio's detector is an Indigo Systems InSb 320x256 pixel chip with 30 micron pixels on an ISC9809 readout. This chip is in the process of being integrated with SDSU (a.k.a. Leach) electronics, rather than the Indigo Systems electronics for full desired functionality. Indigo Systems specifications give the detector's dark current as $6.2\text{x}10^6$ e-/s at 77 K. The readout has two selectable gain values that switch between two different modes of the chip. The high gain mode has a readnoise of 70 e- and a full well depth of $0.17\text{x}10^6$ e-, while the low gain mode has a readnoise of 700 e- and a full well depth of $3.5\text{x}10^6$ e-. The chip has 4 outputs than can each clock at approximately 1 MHz with the SDSU electronics. This chip was chosen because its specifications give good performance in the thermal infrared, especially at M band. The high full well depth and fast readout of the chip allow a large field of view relative to other detectors, which saturate quickly in M band. Since the thermal background is the dominant source of noise, the relatively large readnoise is a negligible noise source.

4.3. Dewar and Hardware

The dewar is a dual-vessel system where the external chamber is a simple liquid nitrogen vessel that cools the cold plate on which all of the optics are mounted. The interior vessel is isolated from the rest of the instrument and controls only the detector's temperature. It has the option of pumping on the nitrogen to achieve temperatures below 77K. This may be used to help reduce the high dark current of the detector. A vapor cooled shield has been added around both vessels to increase the hold times.

4.4. Status

The dewar is currently being machined and assembled by IRLabs in Tucson, AZ and will be completed in August of 2004. Testing on the detector is ongoing. We plan to commission Clio with the MMT adaptive secondary in Fall 2004-Winter 2005.

5. SENSITIVITY ANALYSIS

5.1. Filter Choice

To choose the best filters in the thermal IR for exoplanet detection, we calculated the signal-to-noise (S/N) in a series of filters for model exoplanets with two hour integrations on the MMT with the exoplanets placed at a distance of 10 pc. This was done for 34 exoplanets using theoretical spectral models from Burrows, Sudarsky, and Lunine (2003)[10] and Sudarsky, Burrows, and Hubeny (2003).[11] The 32 exoplanet models from Burrows, Sudarsky, and Lunine (2003) are equilibrium models that ignore stellar radiation and have masses ranging from 1-25 M_{Jupiter} and ages ranging from 100 Myr - 5 Gyr. The final two exoplanet models from the work of Sudarsky, Burrows, and Hubeny (2003) take stellar radiation into consideration. These latter two models are predictions for spectra of 55 Cnc d, an exoplanet detected by radial velocity methods (4.05 M_{Jupiter} at 5.9 AU from its 5 Gyr old G8V primary), and a 10 M_{Jupiter} exoplanet orbiting its G0V primary star at 10 AU with an age of 1 Gyr. Signal-to-noise values were calculated for a set of filters with central wavelengths from 2.5-5.5 microns in intervals of 0.05 microns and widths of 0.02-1.2 microns in intervals of 0.02 microns. Filters were modelled by a boxcar shape with a maximum transmission of 85% and a minimum transmission of 0%. The following noise sources were taken into consideration:

- Throughput of the Telescope (primary and secondary Aluminum mirrors) + Adaptive Optics (no extra optics) + Clio (dichroic window, ZnSe AR coated lens, Gold mirror, filter, Cleartran AR coated lens, Gold mirror, chip).
- Atmospheric absorption of Mauna Kea (1.2 mm water column; produced using the program IRTRANS4 and obtained from the UKIRT worldwide web pages)

- Sky background (1.0 mm water column).[17]
- Telescope emissivity of 10%. Measurements of the telescope emissivity at the MMT with the adaptive secondary give 6.5%. We have chosen 10% as a conservative value.
- Strehl ratio. Values achievable at the MMT system were assumed (40% at H band with vibrations removed; equivalent to 81% at L and 87% at M).
- Photon noise from the exoplanet signal.
- Detector dark current and readnoise (see Section 4.2).
- Photon and speckle noise from the primary star was ignored here for simplicity and will be addressed in the following section. This is valid for exoplanets at large separations from their primary stars, where the

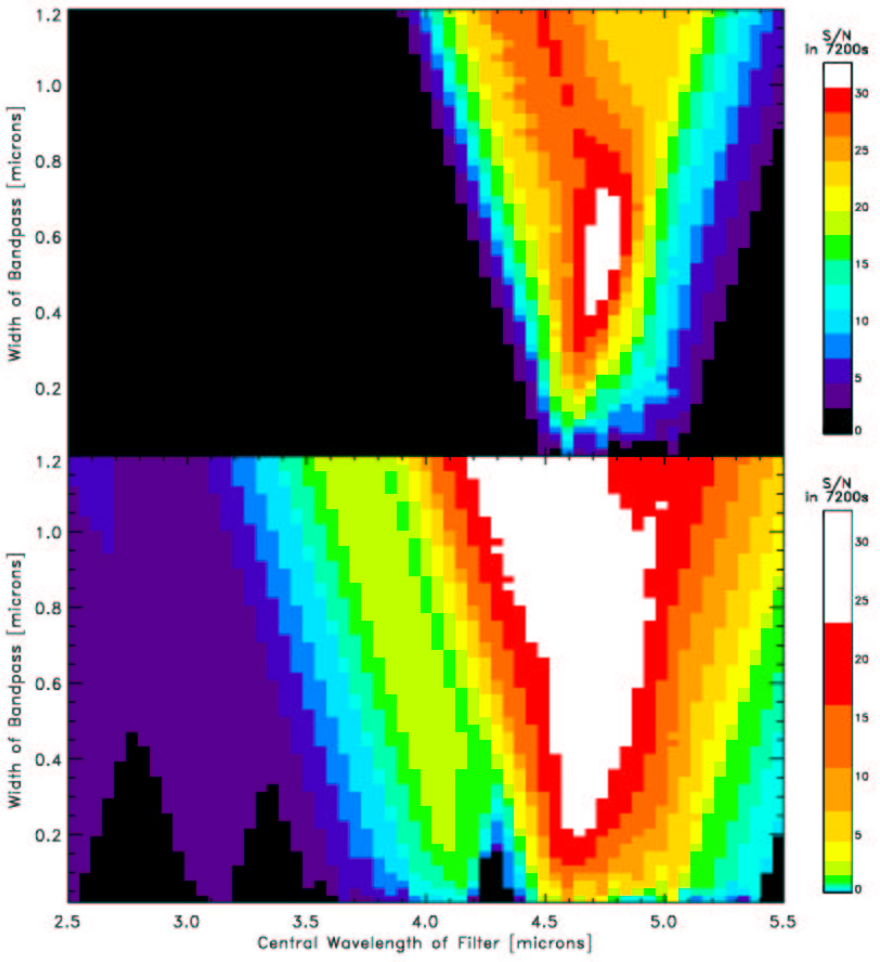

Figure 3. Results of filter choice analysis for a two hour integration at the MMT of a 55 Cnc d type system placed at 10 pc. Theoretical models were taken from Sudarsky, Burrows, and Hubeny (2003). The best filter for detection has a central wavelength near 4.75 microns and a width near 0.58 microns. (top) linear scaling to see best filter (bottom) 6th root scaling to see low signal-to-noise areas.

speckle and photon noise from the point spread function (PSF) become negligible relative to other noise sources.

Figure 3 shows the results of this analysis for a 55 Cnc d type system placed at 10 pc. Note that we show this exoplanet because the model includes the effects of stellar irradiation and it is similar to the least massive, oldest planet we expect to detect with Clio. The best filter for detection was chosen by considering lower mass, older planets more strongly since they are more difficult to detect. The optimum chosen filter has a central wavelength of approximately 4.75 microns and a width of 0.58 microns.

5.2. Full Sensitivity Calculation

Here, we add photon and speckle noise from the primary star to the calculation to produce sensitivity curves for the filter chosen in the previous section. To do this, we have carried out monochromatic, temporally uncorrelated AO simulations where the atmosphere is simulated by seven discreet layers. The properties and number of layers are based on a set of SCIDAR measurements taken at Mt. Graham and Mt. Hopkins in Arizona.[18] For each atmospheric layer we have created a series of independent, random, phase screens with Kolmogorov statistics as described by Noll (1976).[19] The noiseless shape of the deformable mirror (DM) was calculated using a reconstructor matrix typical of that used for the MMT AO system. The following noise sources were included in the AO simulation:

- Simulation fitting error. There is a limit to how well we can model the atmosphere because only the first 496 Zernike modes can be calculated using double precision. Modes 497 through 5151 were calculated using an arbitrary precision algorithm so that the residual fitting error was only $\sigma^2_{\text{sim fit}} = 0.00165004$ rad^2.
- Actuator fitting error. Fitting error due to the finite number of actuators on the DM is accounted for by the fact that our reconstructor only calculates the DM shape using the first 54 Zernike modes.
- Reconstructor error. Photon noise from the primary star and sky background as well as detector readnoise and dark current all contribute to noise in the wavefront reconstruction. These errors have been included by propogating them through the linear system represented by the reconstructor and adding them to the uncorrected wavefront phase.
- Control loop time delay. The contribution of time delay to the error in each Zernike mode on the DM was calculated by examining the behavior of the Zernike coefficients versus time using the temporal power spectrum formulated by Roddier (1999).[20] For each Zernike mode, the coefficient value was calculated versus time for a time delay of 41 ms. The standard deviation of the differences between numerous (∼80000) pairs of coefficients, separated by that delay, was taken as the time delay error for that Zernike mode. Examination of the distribution of the differences showed that they were consistent with a gaussian. These random errors were then added to the uncorrected wavefront phase.

The above simulations produced a series of temporally uncorrelated residual phase screens that were then propogated through a Fourier optics model of Clio and added together to produce a time-averaged PSF. This PSF was then used to calculate the photon noise from the exoplanet's primary star. In order to estimate the speckle noise from the stellar PSF, the speckle noise formulation from Racine et al. (1999)[21] was used:

$$\sigma^2_{\text{speckle}} = \frac{\text{Number of Photons in Speckle}^2}{16\ (\text{Speckle Lifetime})}$$

This method was preferred over a time-correlated AO model because of the extreme computational intensity required for an appropriate simulation of a two hour observation and, more importantly, the fact that atmospheric speckles are known to underestimate the amount of observed speckle noise (i.e. they ignored super-speckles). Since the source of super-speckles is currently unknown, there are no models that are able to accurately reproduce them. As a result, we have chosen to use the above formula and explored several different speckle lifetime values (0.1, 1, 10, 100, 1000 seconds) to cover a reasonable range of speckle noise.

To try and understand which of these speckle lifetimes was most reasonable for the MMT, we examined data taken in the L band with MIRAC/BLINC (at the MMT) and found that the typical speckle lifetime was about 4 seconds. This was determined by calculating the total error in a 10 s stellar image as a function of radius, subtracting off all other noise sources, scaling to a 2 hour integration, and plotting on an equivalent plot to Figure 4 (described below) for L band. Since the MIRAC/BLINC image was only 10 s long, it may not have had enough time to record the full duration of a super speckle. As a result, the estimation is most likely a lower limit to the actual speckle lifetime of a long exposure image. More observations are necessary to determine the true speckle lifetime with the MMT AO system, however we can impose an upper limit on the effective speckle lifetime by rotating the instrument during observations. We can achieve an approximately 90% observing efficiency while rotating the instrument every 100 s of integration. Therefore, a reasonable range of actual speckle lifetimes for the MMT AO system is approximately 4-100 s.

The estimated photon and speckle noise of a 1 Gyr old G0V primary star at 10 pc was then calculated to produce a sensitivity vs. separation plot (see Figure 4) for the filter chosen in section 5.1. Figure 5 shows a breakdown of contributions from each of the individual noise sources. Speckle noise and thermal background

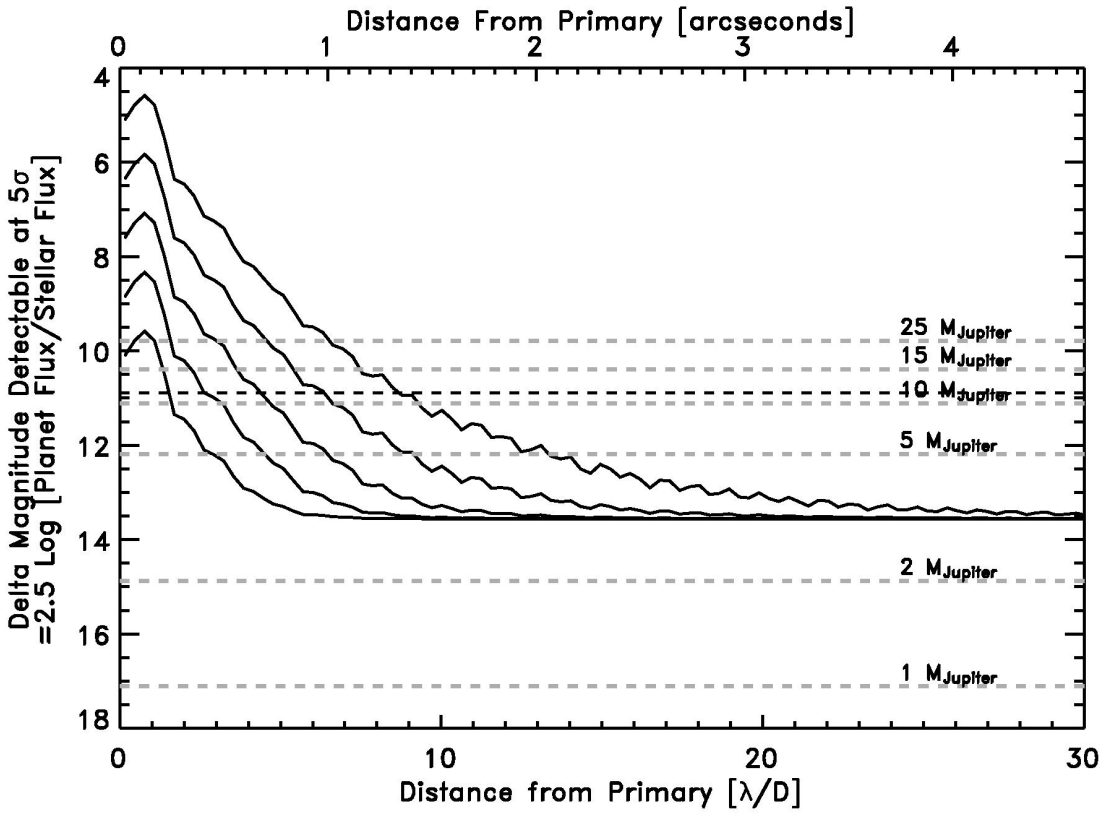

Figure 4. Results of Clio sensitivity analysis for filter with central wavelength of 4.75 microns and width of 0.58 microns (note AO simulations were monochromatic). The solid lines show the sensitivity estimates for five different values of speckle lifetimes. Speckle lifetimes of 0.1, 1, 10, 100, and 1000 seconds were assumed, where the top-most solid line is for 0.1 second. Any exoplanets on the plot lying above these sensitivity lines are detectable. The primary star is assumed to be a G0V ($\sim 1\ M_{\odot}$) at 10pc and 1 Gyr old. The black dotted line shows where an irradiated 10 $M_{\rm Jupiter}$ exoplanet 10 AU from the primary star would lie on the plot.[11] Therefore, we would expect to be able to detect this type of exoplanet at separations larger than 1.5 λ/D (0.2") from the primary star for a speckle lifetime of 0.1 s and 8.7 λ/D (1.3") for a speckle lifetime of 1000 s. A series of 1 Gyr old isolated planet models from Burrows, Sudarsky, and Lunine (2003) are also included on the plot as grey dashed lines.

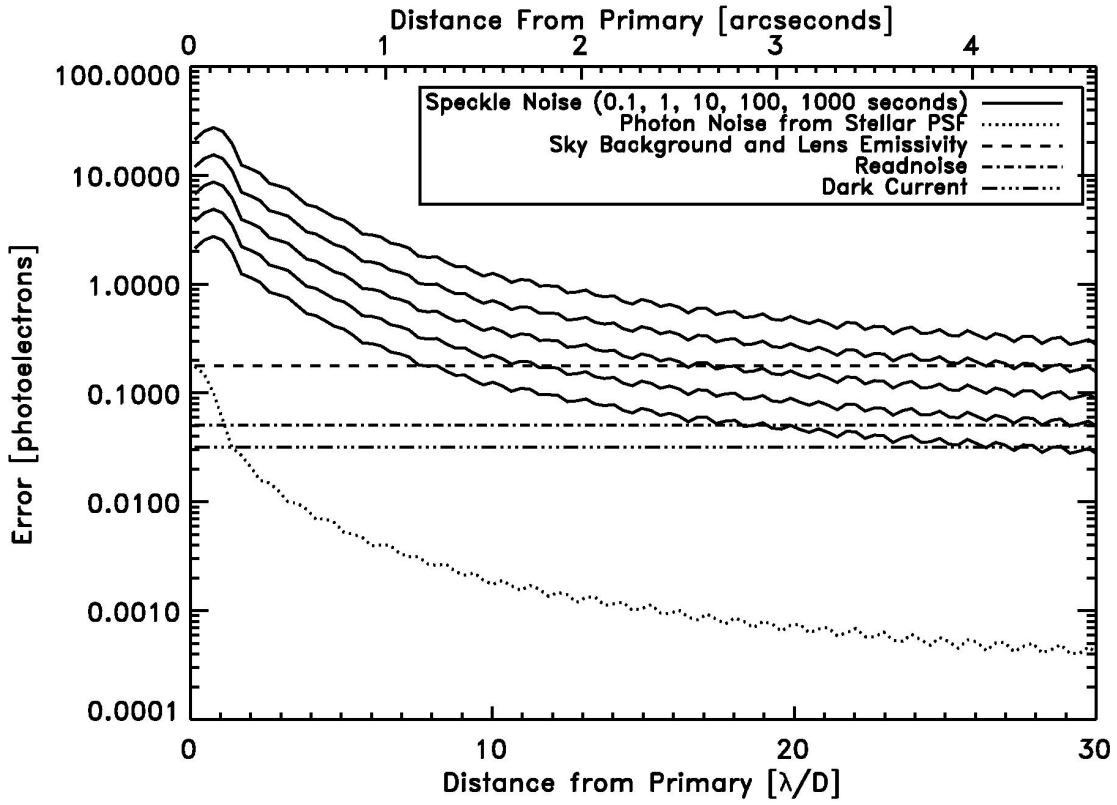

Figure 5. Contribution of different noise sources to the overall noise of Clio. Values are for a two hour integration on the MMT on a 1 Gyr old G0V star at 10 pc. The filter used has a central wavelength of 4.75 microns and a width of 0.58 microns. Notice that the dominant noise sources are i) speckle noise; and ii) sky background/lens emissivity. Photon noise of the stellar psf is negligible while detector noise is small.

are the dominant noise sources, while photon noise of the stellar PSF is negligible. The noise associated with a PSF subtraction of a similar star is also included in Figure 4, but not shown in Figure 5. The sensitivity plot (Figure 4) shows that we expect to detect a 5 $M_{\rm Jupiter}$ exoplanet further out than about 2.9 diffraction widths (0.45") for a speckle lifetime of 0.1 s and further out than about 13.4 λ/D (2.1") for a speckle lifetime of 1000 s. Similarly, we expect to detect a 15 $M_{\rm Jupiter}$ exoplanet further out than approximately 1.3-7.5 λ/D (0.2-1.2").

5.3. Coronography In The Thermal IR

The above analysis has shown that the dominant sources of noise, in the thermal IR, for companion detection are speckle noise and thermal background (see Figure 5). Photon noise from the stellar PSF is an insignificant contributor to the overall noise of the system. As a result, supression of the stellar PSF with a coronograph is of little use in so far as it reduces the photon noise from the stellar PSF. However, there is some indication that coronography may be useful in reducing speckle noise where components of the PSF that are modulated by the diffraction-limited core dominate (i.e. "pinned" speckles).[22] For Clio, we will be using an obscured, unapodized primary with Strehl ratios of approximately 85% in M band. For this type of system, we would expect a coronograph to be useful at very close separations, where the "pinned" PSF terms would dominate.[22] Since Clio's sensitivity is dominated by speckle noise close in, but not further out, coronography may be of particular use in improving sensitivity at very close separations.

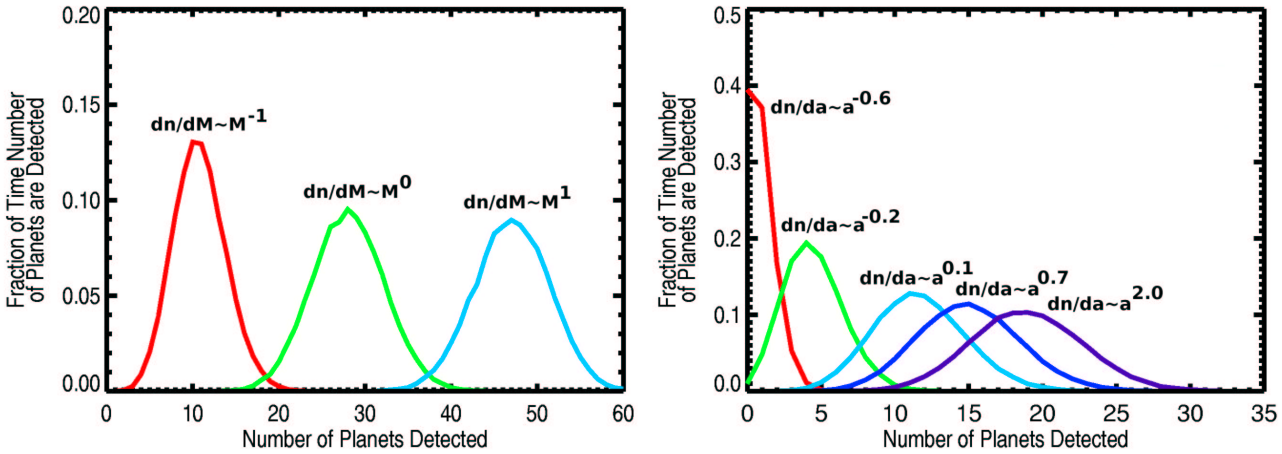

Figure 6. (left) Fractional chance of detecting various numbers of planets given a separation distribution function of $dn/da \sim a^{0.7}$ and three different mass distribution functions for planets. All three mass distributions are clearly distinguishable. (right) Fractional chance of detecting various numbers of planets given a mass distribution of $dn/dM \sim M^{-0.7}$ and 5 different separation distribution functions. It appears unlikely that no planets will be detected with this survey. If, indeed, no planets are detected, we should be able to rule out a significant region of parameter space for these distribution functions.

6. EXOPLANET SURVEY

Given our expected sensitivity and what is currently known about exoplanets, we have run a series of Monte Carlo simulations to understand what we expect to see with Clio. These results will be used to constructed a survey that has the ability to provide statistical information about the exoplanet population, even for a null result.

Radial velocity surveys provide a baseline from which we can make predictions about the distribution of exoplanets at further separations from their primaries. Current results indicate a companion mass distribution of $dn/dM \sim M^{-0.7}$ and a separation distribution of $dn/da \sim a^{>-1}$ (Marcy et al. 2003[1]). A fit to the data (for 0.2 AU $<$ a $<$ 2 AU) gives $dn/da \sim a^{0.7}$ as a starting point. Our survey will enable a quantitative test of the hypothesis that the mass and separation distributions of outer planets are consistent with those observed within 5 AU.

As a first hypothesis to test, we can simply extend the observed distributions to larger separations. We performed a series of Monte Carlo simulations where the radial velocity mass distribution was taken to be valid from 1-15 $M_{\rm Jupiter}$ and the separation distribution was extended from 0.01-50 AU. An outer boundary of 50 AU was chosen to be consistent with the outer edge of our Kuiper Belt[23] as well as the radius of the smallest silhouette disk in Orion.[24] Estimates of our sensitivities versus separation from the central star are derived in section 5.2. We are using the estimates for a speckle lifetime of 100 s here as a conservative estimate. Note that these sensitivity estimates assume equilibrium exoplanet models. Further investigation of non-equilibrium models below 700 K is needed to determine the strength of the effect of increased CO absorption from 4.5-5 microns for our targets.

These simulations were used to define an optimal survey sample of 80 M0-F0 stars within 20 pc and less than 1 Gyr old. With this sample, and assuming $dn/da \sim a^{0.7}$ and $dn/dM \sim M^{-0.7}$, we expect to detect 15±3 companions with 4-15 $M_{\rm Jupiter}$ at 17-50 AU.

We do not necessarily expect our simple extrapolation to be valid given that at very small separations planets may have very different evolutionary histories than their larger separations counterparts (e.g. planet migration after formation[25, 26]). Our survey will provide an indication of the shape of the separation and mass distribution functions based on the number of companions detected.

Figure 6 indicates our chances of detecting various numbers of planets given $dn/da \sim a^{0.7}$ as well as three different planet mass distribution functions of the form $dn/dM \sim M^{\alpha}$ with α=[-1,0,1]. These three distribution functions are clearly distinguishable for the given sample. Assuming the given separation distribution function, we would be able to rule out $dn/dM \sim M^{-1}$ at 4σ and $dn/dM \sim M^{1}$ at 11σ in the event of no planet detections.

The same process can be repeated for various separation distributions. Figure 6 indicates our chances of detecting various numbers of planets, while this time keeping $dn/dM \sim M^{-0.7}$ and varying the separation distribution function from $dn/da \sim a^{\beta}$ β=[-0.6,-0.2,0.1,0.7,2]. For a null result we can rule out β=-0.2 at 2σ and β=0.7 at 4σ.

These limits will provide valuable constraints on theories of planet formation and evolution as well as help guide the next generation of direct detection surveys.

ACKNOWLEDGMENTS

We would like to thank IRLabs for their expert help, especially Elliott Solheid for designing the instrument dewar, Ken Salvestrini for helping with the detector testing, Mitch Nash for machining the parts, Kirby Hnat for doing the thermal analysis, and Ron Dewitt for helping with the dewar design. Thanks also to Michael Lesser for helping us integrate AZCam with Clio, Dave Sudarsky for slaving over the 10 $M_{\rm Jupiter}$ model and answering all our model questions, John Codona for insightful discussions on speckle noise, Patrick Young for providing his pre-main sequence stellar models, and Dick Joyce for helping with filter measurements. M.Freed acknowledges support from the NASA Graduate Student Researchers Program (NGT5-50394). We also acknowledge support from the TPF Foundation Science Program, AFOSR, and the NASA Astrobiology Institute "Laplace Center" node at the UofA.

REFERENCES

1. G. Marcy, P. R. Butler, D. A. Fischer, and S. S. Vogt, "Properties of extrasolar planets," in *Scientific Frontiers in Research on Extrasolar Planets*, D. Deming and S. Seager, eds., *ASP Conf. Ser.* **294**, pp. 1–16, 2003.
2. D. Charbonneau, T. M. Brown, D. W. Latham, and M. Mayor, "Detection of planetary transits across a sun-like star," *ApJ* **529**, pp. L45–L48, 2000.
3. D. Charbonneau, T. M. Brown, R. W. Noyes, and R. L. Gilliland, "Detection of an extrasolar planet atmosphere," *ApJ* **568**, pp. 377–384, 2002.
4. M. Konacki, G. Torres, S. Jha, and D. D. Sasselov, "An extrasolar planet that transits the disk of its parent star," *Nature* **421**, pp. 507–509, 2003.
5. F. Bouchy, F. Pont, N. C. Santos, C. Melo, M. Mayor, D. Queloz, and S. Udry, "Two new very hot jupiters among the ogle transiting candidates," *A&A* **submitted**, 2004.
6. M. Konacki and et al., "The transiting extrasolar giant planet around the star ogle-tr-113," *ApJ* **609**, pp. L37–L40, 2004.
7. A. Burrows, M. Marley, W. B. Hubbard, J. I. Lunine, T. Guillot, D. Saumon, R. Freedman, D. Sudarsky, and C. Sharp, "A nongray theory of extrasolar giant planets and brown dwarfs," *ApJ* **491**, pp. 856–875, 1997.
8. G. Chabrier, I. Baraffe, F. Allard, and P. Hauschildt, "Evolutionary models for very low-mass stars and brown dwarfs with dusty atmospheres," *ApJ* **542**, pp. 464–472, 2000.
9. M. S. Marley, S. Seager, D. Saumon, K. Lodders, A. S. Ackerman, R. S. Freedman, and X. Fan, "Clouds and chemistry: Ultracool dwarf atmospheric properties from optical and infrared colors," *ApJ* **568**, pp. 335–342, 2002.
10. A. Burrows, D. Sudarsky, and J. I. Lunine, "Beyond the t dwarfs: Theoretical spectra, colors, and detectability of the coolest brown dwarfs," *ApJ* **596**, pp. 587–596, 2003.
11. D. Sudarsky, A. Burrows, and I. Hubeny, "Theoretical spectra and atmospheres of extrasolar giant planets," *ApJ* **588**, pp. 1121–1148, 2003.

12. D. A. Golimowski, S. K. Leggett, M. S. Marley, X. Fan, T. R. Geballe, G. R. Knapp, F. J. Vrba, A. A. Henden, C. B. Luginbuhl, H. H. Quetter, J. A. Munn, B. Canzian, W. Zheng, Z. I. Tsvetanov, K. Chiu, K. Glazebrook, E. A. Hoversten, D. P. Schneider, and J. Brinkmann, "L' and m' photometry of ultracool dwarfs," *AJ* **127**, pp. 3516–3536, 2004.
13. D. Saumon, M. S. Marley, K. Lodders, and R. S. Freedman, "Non-equilibrium chemistry in the atmospheres of brown dwarfs," in *Brown Dwarfs*, E. Martín, ed., *Proc. of IAU Symp.* **211**, p. 345, 2003.
14. M. Lloyd-Hart, "Thermal performance enhancement of adaptive optics by use of a deformable secondary mirror," *PASP* **112**, pp. 264–272, 2000.
15. F. P. Wildi, G. Brusa, and M. Lloyd-Hart, "First light of the 6.5-m mmt adaptive optics system," in *Astronomical Adaptive Optics Systems and Applications*, R. K. Tyson and M. Lloyd-Hart, eds., *Proc. SPIE* **5169**, pp. 17–25, 2003.
16. G. Brusa-Zappellini, A. Riccardi, F. P. Wildi, M. Lloyd-Hart, H. M. Martin, R. Allen, D. L. Fisher, D. L. Miller, R. Biasi, D. Gallieni, and F. Zocchi, "Mmt adaptive secondary: first ao closed-loop results," in *Astronomical Adaptive Optics Systems and Applications*, R. K. Tyson and M. Lloyd-Hart, eds., *Proc. SPIE* **5169**, pp. 26–36, 2003.
17. F. C. Gillett and M. Mountain, "On the comparative performance of an 8m ngst and a ground based 8m optical/ir telescope," in *Science with the Next Generation Space Telescope*, *ASP Conf. Ser.* **133**, p. 42, 1998.
18. D. L. McKenna, R. Avila, J. M. Hill, S. Hippler, P. Salinari, P. C. Stanton, and R. Weiss, "Lbt facility scidar: recent results," in *Adaptive Optical System Technologies II*, P. L. Wizinowich and D. Bonaccini, eds., *Proc. SPIE* **4839**, pp. 825–836, 2003.
19. R. J. Noll, "Zernike polynomials and atmospheric turbulence," *J. Opt. Soc. Am.* **66**, pp. 207–211, 1976.
20. F. Roddier, *Adaptive Optics in Astronomy*, Cambridge University Press, Cambridge, UK, 1999.
21. R. Racine, G. A. H. Walker, D. Nadeau, R. Doyon, and C. Marois, "Speckle noise and the detection of faint companions," *PASP* **111**, pp. 587–594, 1999.
22. M. D. Perrin, A. Sivaramakrishnan, R. B. Makidon, B. R. Oppenheimer, and J. R. Graham, "The structure of high strehl ratio point-spread functions," *ApJ* **596**, pp. 702–712, 2003.
23. C. A. Trujillo and M. E. Brown, "The radial distribution of the kuiper belt," *ApJ* **554**, pp. L95–L98, 2001.
24. J. Bally, C. R. O'Dell, and M. J. McCaughrean, "Disks, microjets, windblown bubbles, and outflows in the orion nebula," *AJ* **119**, pp. 2919–2959, 2000.
25. P. J. Armitage, M. Livio, S. H. Lubow, and J. E. Pringle, "Predictions for the frequency and orbital radii of massive extrasolar planets," *MNRAS* **334**, pp. 248–256, 2002.
26. D. E. Trilling, J. I. Lunine, and W. Benz, "Orbital migration and the frequency of giant planet formation," *A&A* **394**, pp. 241–251, 2002.